NUMERICAL STUDY ON TURBULENT BUBBLY FLOW IN VERTICAL CHANNEL

Fang-Yu Chen
Department of Engineering Mechanics
Tsinghua University
Beijing 100084, China
Chen-fy20@mails.tsinghua.edu.cn

Wei-Xi Huang
Department of Engineering Mechanics
Tsinghua University
Beijing 100084, China
hwx@tsinghua.edu.cn

Chun-Xiao Xu
Department of Engineering Mechanics
Tsinghua University
Beijing 100084, China
xucx@tsinghua.edu.cn

ABSTRACT

Bubbly flows are prevalent in both natural environments and industrial fields, and have been proven to be effective in turbulent drag reduction. Direct numerical simulation with two-way coupled Lagrange tracking is used to study the distribution of bubbles and the modulation of turbulence. All simulations are conducted in an upward vertical turbulent channel. The flow is driven by a constant pressure gradient, corresponding to a friction Reynolds number $Re_{\tau 0} = 180$. Six bubble diameters ($d = 120{\sim}240\mu m$) are considered. Significant bubble accumulation close to the wall is observed, primarily due to the lift force acting on bubble. Bubbles exhibit three different preferential concentration patterns in the *x*-*z* plane along the wall-normal direction. Two mechanisms are proposed for this phenomenon. Furthermore, the small bubble leads to a reduction in bulk velocity, decreasing the velocity profile and terms in turbulent kinetic energy budget, while the profile of the large bubble almost overlaps that of the unladen flow. The turbulence modulation is founded highly restricted across all the bubble size. The impact of the bubble is almost the same as the increasing mean pressure gradient in the single-phase flow.

INTRODUCTION

Turbulent bubbly flows are frequently encountered in environmental and industrial scenarios, such as gas realising in ocean, bubble columns and heat exchange units. Bubbles in turbulent boundary layers cause modulation in turbulent structures, leading to drag reduction. Kato et al. (2000) highlighted those large bubbles enhance turbulence, whereas small bubbles attenuate turbulence. Villafuerte and Hassan (2006) pointed out that bubble accumulation near the wall, particularly in the buffer layer, leads to drag reduction. The distribution of bubbles in wall-bounded turbulence is complicated, Park et al. (2019) observed that microbubbles prefer accumulation in low-speed streaks. Molin et al. (2012) observed strong wall accumulation and preferential concentration in low-speed regions in upflow, while in high-speed region in downflow. The Euler–Lagrange (E-L) method is an important tool to study bubble motion and bubble-turbulence interaction. Giusti et al. (2005) conducted one-way coupled E-L simulation to study the bubbly flow in an upflow vertical channel; they emphasized the importance of lift force in near-wall region. Asiagbe et al. (2019) conducted LES simulation at higher Reynolds number, highlighting the importance of pressure gradient force and add-mass force in higher Reynolds number.

However, the physical mechanism underlying the preferential accumulation of bubbles remains unclear, and the mechanisms behind the turbulent drag reduction remain controversial. In this study, direct numerical simulation, together with Lagrange tracking, is used to simulate microbubbles in upward vertical turbulent channel. The aim of the present work is to investigate the bubble preferential concentration, study the dynamics characteristics of bubble, and analyze the turbulence modulation by bubble.

NUMERICAL APPROACH

The governing equations for the incompressible Newtonian fluid are the continuity equation and the Navier-Stokes equations, i.e.

$$\frac{\partial u_i}{\partial x_i} = 0 \tag{1}$$

$$\frac{\partial u_i}{\partial t} + u_j \frac{\partial u_i}{\partial x_j} = -\frac{1}{\rho_f}\frac{\partial p}{\partial x_i} + \nu \frac{\partial^2 u_i}{\partial x_j \partial x_j} + \frac{1}{\rho_f}\frac{P_0}{dx}\delta_{1,i} + \frac{f_i}{\rho_f} \tag{2}$$

Eqs. (1) and (2) are numerically solved using the finite difference method based on a projection method proposed by Kim et al. (2002). The code employs fully implicit time advancement and has 2nd-order temporal and spatial accuracies. A constant pressure gradient is imposed to drive the flow, which corresponds to the friction Reynolds number $Re_{\tau 0} = 180$. The domain size is $4\pi h \times 2h \times 2\pi h$, with a channel half width $h = 0.036m$. The number of grid points are $(N_x, N_y, N_z) = (384,128,256)$. The gravity is along the negative streamwise direction. The detail of the computational domain is shown in Figure 1.

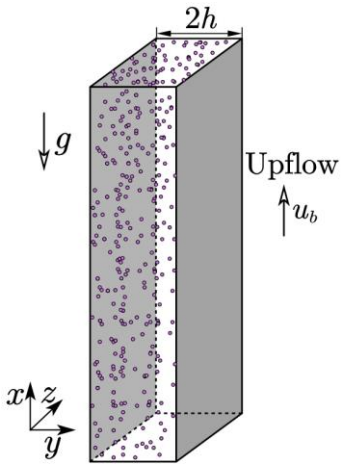

Figure 1. Sketch of the computational domain

The bubbles are tracked by solving Eqs. (3) and (4), which include gravity/buoyancy force, drag force, lift force, wall-lift force, pressure gradient force, added mass force and basset force. A 2nd-order Adams-Bashforth scheme is employed for time advancement of individual bubbles. Interpolation of fluid properties at the bubble position is performed using 5th-order Hermite polynomials. At the beginning of simulation, bubbles are uniformly injected into a fully developed single-phase flow, with the bubble velocity equal to the fluid velocity at bubble position.

$$\frac{\mathrm{d}\mathbf{x_b}}{\mathrm{d}t}=\mathbf{u_b} \tag{3}$$

$$\begin{aligned}\frac{\mathrm{d}\mathbf{u_b}}{\mathrm{d}t}&=\mathbf{F}_G+\mathbf{F}_D+\mathbf{F}_L+\mathbf{F}_P+\mathbf{F}_A+\mathbf{F}_W+\mathbf{F}_B\\&=\left(1-\frac{\rho_f}{\rho_b}\right)\mathbf{g}+C_D\frac{3}{4d}\frac{\rho_f}{\rho_b}|\mathbf{u_b}-\mathbf{u_{@b}}|\left(\mathbf{u_b}-\mathbf{u_{@b}}\right)\\&+C_L\frac{\rho_f}{\rho_b}\left(\mathbf{u}-\mathbf{u_b}\right)\times\left(\nabla\times\mathbf{u}\right)+C_W\frac{\rho_f}{\rho_b}\frac{2}{d}|u_{sw}|^2\,\mathbf{e}_y\\&+\frac{\rho_f}{\rho_b}\frac{\mathrm{D}\mathbf{u_{@b}}}{\mathrm{D}t}+C_M\frac{\rho_f}{\rho_b}\left(\frac{\mathrm{D}\mathbf{u_{@b}}}{\mathrm{D}t}-\frac{\mathrm{d}\mathbf{u_b}}{\mathrm{d}t}\right)\\&+C_B\int_{-\infty}^{t}K_B(t-\tau)\left(\frac{\mathrm{d}\mathbf{u_{@b}}}{\mathrm{d}t}-\frac{\mathrm{d}\mathbf{u_b}}{\mathrm{d}t}\right)\mathrm{d}\tau\end{aligned} \tag{4}$$

A two-way coupling between bubble and fluid is considered, and the feedback of bubble to fluid is the source term f_i in Eq. (2), which is the sum of all forces in Eq. (4) without the gravity/buoyancy force, i.e.

$$\mathbf{f}=-\frac{1}{6}\rho_b\pi d^3\left[\frac{\mathrm{d}\mathbf{u_b}}{\mathrm{d}t}-\left(1-\frac{\rho_f}{\rho_b}\right)\mathbf{g}\right] \tag{5}$$

In the present simulations, the bubble diameters are $d=[120,125,130,140,180,240]\mu m$, while the volume fraction is $\alpha_v=3\times10^{-5}$ for all the cases. The bubble-bubble interaction is neglect because $\alpha_v<1\times10^{-3}$ (Elghobashi, 1994). The bubble Stokes number $St=\tau_b/\tau_f$ ranges from 0.014 to 0.057. Table 1 shows the details of the bubble parameters. The bubble Froude number is defined as $Fr=\left[u_\tau^3(\rho_b+0.5\rho_f)\right]/\left[\nu g(\rho_f-\rho_b)\right]$. Although $St\ll1$ means the bubble could response rapidly to the fluctuation of fluid, however bubble cannot be considered as tracer particle because that for $St/Fr\sim O(1)$, the effect of buoyancy force plays an important role in bubble dynamics (Mathai et al., 2020). The Eotvos number $Eo\ll1$, so the bubble can be considered as a rigid sphere (Clift et al., 1978).

Table 1. Computational parameters of bubble

$d(\mu m)$	d^+	St	St/Fr	N_b
120	0.72	0.014	1.3	244289
125	0.75	0.015	1.4	216132
130	0.78	0.017	1.5	192140
140	0.84	0.019	1.8	153838
180	1.07	0.032	3.0	72382
240	1.43	0.057	5.3	30536

RESULTS AND DISCUSSION

In upflow, the buoyancy force of the bubble drives the flow to acceleration, resulting in an increase in bulk velocity and wall shear (Molin et al., 2012). The effective friction Reynolds number considering the bubble-induced flowrate modification is $\mathrm{Re}_\tau=\mathrm{Re}_{\tau0}\left[1+\alpha_v\left(1-\rho_b/\rho_f\right)g^+\right]\approx214.7$, which is the same for all the bubble-ladden cases. To eliminate the Reynolds number effect between bubble-ladden flow and unladen single-phase flow, the mean pressure gradient of unladen flow is increased to obtain a same frction Reynolds number Re_τ as bubble-ladden flow.

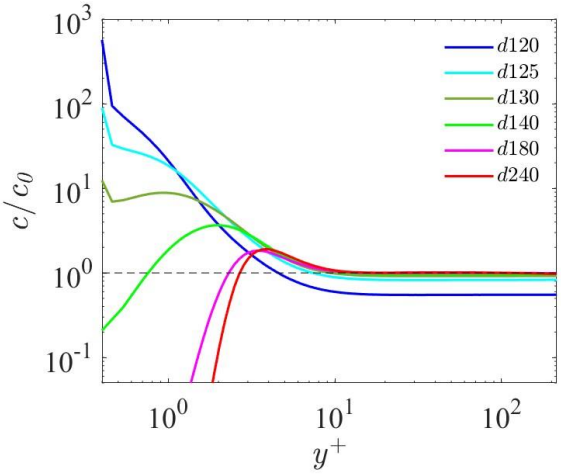

Figure 2. Bubble number density distribution, normalized by mean bulk number density c_0

Figure 2 shows the bubble number density distribution c, normalized by the mean bulk number density c_0. two distinct types of bubble number density distribution are observed. Small bubbles ($d\le130\mu m$) are trapped along the wall by the lift force, resulting a monotonic spike of distribution in wall. The highest density peak is observed in the case of

$120\mu m$ bubble, with $c/c_0 \approx 800$. As the bubble diameter increases, the monotonic spike on the wall weakens and a secondary peak appears. This is because the ratio between the wall-lift force and the lift force increases with the diameter of the bubble. Large bubble ($d > 130\mu m$) are driven away from the wall by wall-lift force, the density peak near the equilibrium position of the two forces, approximately two to three times the bubble diameter. In the region $y^+ > 10$, the lift force and wall-lift force decrease rapidly with increasing of wall distance, the density distribution c converges gradually.

Figure 3 shows the mean streamwise fluid velocity $\langle u\rangle^+$, bubble velocity $\langle u_b\rangle^+$ and fluid velocity at bubble position $\langle u_{@b}\rangle^+$. The mean velocity profile $\langle u\rangle^+$ of the $120\mu m$ bubble case is lower than the unladen flow, while the profiles of large bubbles collapse onto the unladen flow almost perfectly. The mean bulk velocity u_m of $120\mu m$ bubble is also lower than the unladen flow, which implies drag increasing.

Due to the buoyancy force acting on the bubble, the bubble velocity $\langle u_b\rangle^+$ is always higher than that of flow and increases with bubble diameter. The mean streamwise slip velocity can be obtained from $\langle u_s\rangle^+ = \langle u_b\rangle^+ - \langle u_{@b}\rangle^+$. When reaching the steady state, the buoyancy force and drag force are in balance in the streamwise direction. Hence, the mean slip velocity can be approximated as

$$\langle u_s\rangle^+ \approx \sqrt{\frac{4(\rho_f-\rho_b)g^+d^+}{3C_D\rho_f}} \approx \frac{St}{Fr}\frac{1}{f(Re_b)} \qquad (6)$$

where the $f(Re_b)=1+0.15Re_b^{0.687}$ is the Reynolds number correction in drag correlation (Schiller and Naumann 1935). As shown in Eq. (4), the mean slip velocity is directly proportional to St and inversely proportional to Fr. The mean fluid velocity at bubble position $\langle u_{@b}\rangle^+$ can manifest the preferential concentration of bubble. For the $120\mu m$ bubble in buffer layer and viscous sublayer, the $\langle u_{@b}\rangle^+$ is lower than $\langle u\rangle^+$, which indicates that the bubbles tend to aggregate in the low-speed region. However, situation is more intricate for the 180 and 240 μm bubbles. In the buffer layer, the $\langle u_{@b}\rangle^+$ remains lower than $\langle u\rangle^+$, whereas it is higher in the viscous sublayer, suggesting a preference for bubble accumulation in the high-speed region within the viscous sublayer.

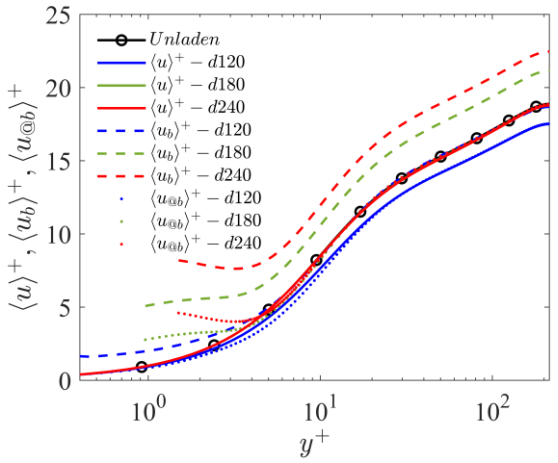

Figure 3. Mean streamwise vlocity profiles of fluid, bubble and fluid at bubble position

Further investigation into preferential concentration has been conducted to better illustrate the phenomenon. In Figure

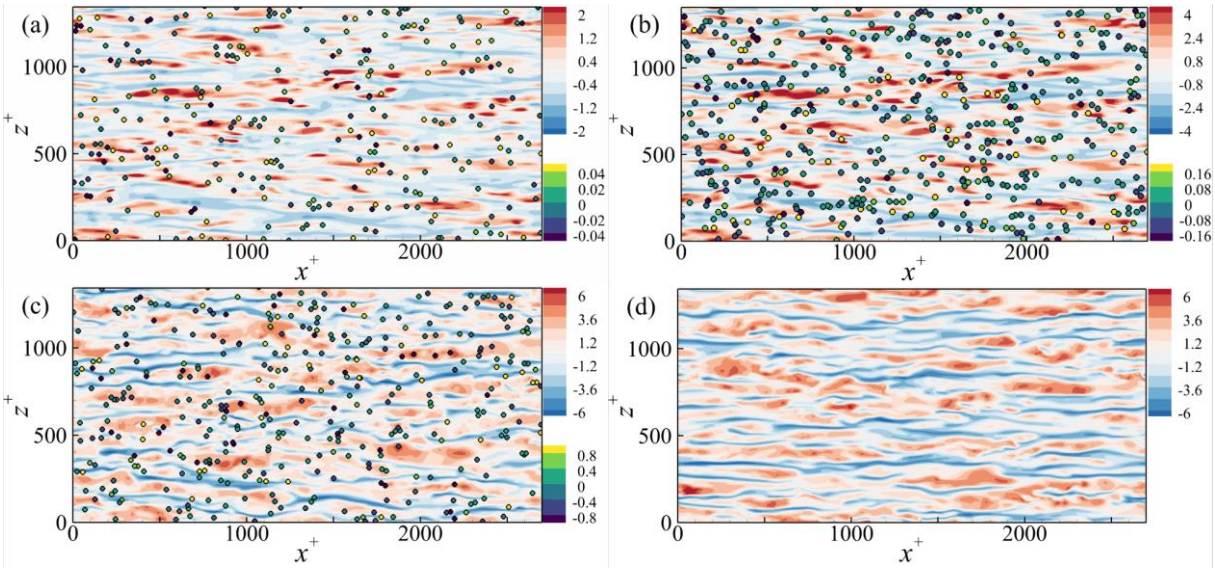

Figure 4. Bubble distribution along the wall-normal direction: (a) $y^+ = 2$; (b) $y^+ = 5$; (c-d) $y^+ = 20$. Contours: instantaneous streamwise fluctuating velocity; circle : bubble position; circle color: bubble wall-normal velocity. (a-c) bubble-laden flow of $d180\mu m$ and (d) single-phase flow

.

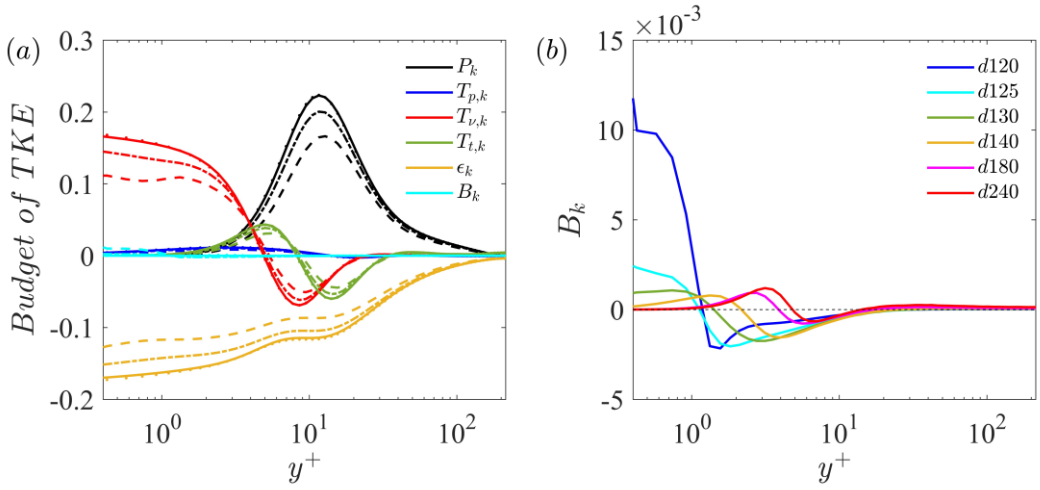

Figure 5. (a) Turbulent kinetic energy budget; (b) bubble-fluid interaction term. Solid: single phase; dashed: $d120\mu m$; dashed-dotted: $d125\mu m$; dotted: $d180\mu m$. In (a) P_k: production; ε_k: viscous dissipation; T_{p_k}: pressure transport ; T_{ν_k}: viscous diffusion; T_{t_k}: turbulent convection; B_k: bubble-fluid interaction .

4, the contours of instantaneous streamwise velocity in the x-z plane together with bubble distribution are shown for the case of $d = 180\mu m$. Three distinct patterns in three regions along the wall-normal direction are revealed: (i) below the peak of bubble concentration which is around $y^+ = 3$, bubbles tend to concentrate in high-speed region as shown in Figure 4(a); (ii) above the peak and below the logarithmic layer, bubbles tend to accumulate in low-speed streaks as shown in Figure 4(b); (iii) within and above the logarithmic layer, bubbles exhibit almost uniform distribution as shown in Figure 4(b).

There are two mechanisms for this phenomenon: Firstly, the sum of lift and wall-lift is positive when bubble position is below the peak, resulting in a positive slip velocity in wall-normal direction. Bubble can be stable only in the fluid region of sweep event where $v < 0$, which is always companied with high speed in the streamwise direction. On the contrary, bubble above the peak will accumulate in the ejection region where $v > 0$. Secondly, the lift force F_L is proportional to the velocity gradient $\partial u/\partial y$, and hence proportional to the streamwise velocity in the viscous sublayer. This means that the bubble in high-speed region will gain larger lift force, and is more likely to be pushed toward the wall, vice versa.

In Figure 4(c,d), compared to the unladen flow, the introduction of $180\mu m$ bubbles exerts only a marginal impact on the flow field. Low-speed streaks are slightly shortened, accompanied by a minor distortion.

To better understand the turbulence modulation by bubbles, the transportation equation of the turbulent kinetic energy (TKE) is analysed:

$$\frac{\partial k}{\partial t} + \langle u_i \rangle \frac{\partial k}{\partial x_i} = P_k + T_{p\_k} + T_{t\_k} + T_{\nu\_k} + \varepsilon_k + B_k \qquad (7)$$

where the bubble-fluid interaction term $B_k = \langle u'_i f_i \rangle$, which is the directly influence of bubble to TKE budget. As shown in Figure 5(a), all the terms in the TKE budget of 120 and 125 μm bubbles are lower than the unladen flow. This is mainly because the TKE in these cases is decreased. The curves converge rapidly with unladen flow, as the bubble diameter increases; when the bubble diameter $d > 130\ \mu m$, the curves nearly overlap. A slight extra suppression is observed in the $120\mu m$ bubble case in viscous dissipation and viscous diffusion terms near the wall. The bubble-fluid interaction term, which is the direct influence of bubble on turbulence, is almost two orders of magnitude lower than the other terms as seen in Figure 5(b).

Table 2 shows the drag increase rate, which is defined as $DI = (C_f - C_{f0})/C_{f0}$, where C_f and C_{f0} are respectively the mean skin friction coefficient of bubble-laden flow and unladen flow. Since the wall shear stress is the same for all the cases, it leads to $DI = u_{m0}^2/u_m^2 - 1$. The case of $120\mu m$ bubble has the largest drag increase, because near half of the bubble are trapped near the wall as shown in Figure 2, resulting in less work done by bubbles on the flow field and a lower mean bulk velocity. The DI is decreased with the increase of bubble diameter. For large bubble ($d_b \geq 140\mu m$), it distributes near uniformly in wall-normal direction, and therefore, only a slight DI is observed.

Table 2. Drag increase rate

$d_b/\mu m$	120	125	130	140	180	240
DI	16.7%	5.9%	3.0%	1.3%	1.1%	1.3%

To better understand the turbulence modulation by bubble and analyse the mechanism of bubble-induced drag increase. We conducted a decomposition of mean skin friction coefficient using the RD identity (Renard and Deck 2016) with an extra bubble-induced term:

$$C_f = C_{f,\nu} + C_{f,t} + C_{f,b}$$
$$= \frac{2}{u_m^3}\left(\int_0^1 \nu \left(\frac{\partial \langle u \rangle}{\partial y} \right)^2 dy + \int_0^1 \overline{-u'v'} \frac{\partial \langle u \rangle}{\partial y} dy + \int_0^1 \left(u_m - \langle u \rangle \right) \langle F_x \rangle dy \right) \quad (8)$$

As shown in Figure 6, the RD identity is based on budget of mean kinetic energy, and comprises three components. The bubble-induced term $C_{f,b}$ reaches its maximum value when the bubble diameter is smallest, gradually converging to zero as the bubble diameter increases. $C_{f,t}$ term represents the energy dissipation of mean flow, and $C_{f,t}$ term represents the energy transfer from mean kinetic energy to turbulent kinetic energy. These two terms exhibit nearly identical behaviour across all bubble-laden flow cases and remain nearly unchanged compared with the unladen flow case.

All the Figures 4, 5, 6 indicate that the turbulence modulation is highly restricted across all cases. The effect of bubble is more likely just injection of energy into the mean flow and the turbulent structures are nearly unchanged. For those large bubbles the introduction of bubble is nearly equivalent to increase the pressure gradient in single-phase flow. This is mainly because the St number in the present bubble-laden study is small $St \sim O(10^{-2})$, and the bubble distributes nearly uniformly in the channel.

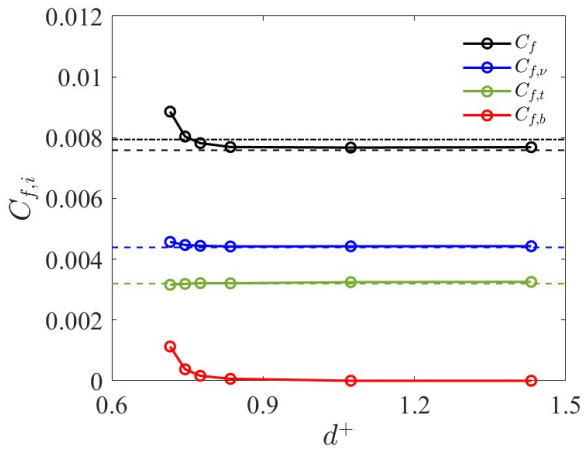

Figure 6. Decompositioni of skin friction coefficient with RD identity. C_f: total mean skin friction coefficient, $C_{f,\nu}$: mean dissipation term, $C_{f,t}$: turbulent kinetic energy production term, $C_{f,b}$: bubble-induced term. Dashed line: each term in unladen flow

CONCLUSION

Bubble distribution and turbulence modulation in vertical turbulent channel were studied by the Euler-Lagrange method with direct numerical simulation. Bubbles exhibit strong accumulation close to the wall due to the lift force, while the wall-lift force prevents bubble from attaching to the wall. Three different patterns of bubble preferential concentration are observed along the wall-normal direction. Two mechanisms of preferential concentration are proposed. The bubble velocity is faster than flow, the mean slip velocity is increased with bubble diameter. The small bubble causes a reduction in the bulk velocity, and decrease of the velocity profile and terms in turbulent kinetic energy budget, while the profile of large bubble is almost close to that of the unladen flow. The turbulence modulation was founded to be highly restricted across all the bubble size especially for large bubble. The effect of bubble injects energy into the mean flow, while the turbulent structures remain nearly unchanged. This is mainly because of the small Stokes number in present study, which results in a nearly uniform distribution of bubble. The impact of bubble is almost the same as increasing the pressure gradient in single-phase flow.

ACKNOWLEDGMENTS

This work was supported by the National Natural Science Foundation of China under Grant Nos. 12272206, 92252204, and 12388101.

REFERENCES

Asiagbe, Kenneth S., Fairweather, Michael, Njobuenwu, Derrick O. & Colombo, Marco 2019 Large eddy simulation of microbubble dispersion and flow field modulation in vertical channel flows. *AIChE Journal* 65 (4), 1325–1339.

Clift, R., Grace, J.R. &Weber, M.E. 1978 Bubbles, Drops, and Particles. London: Whole. Academic Press. Elghobashi, S. 1994 On predicting particle-laden turbulent flows. *Applied Scientific Research* 52 (4), 309–329.

Giusti, Andrea, Lucci, Francesco & Soldati, Alfredo 2005 Influence of the lift force in direct numerical simulation of upward/downward turbulent channel flow laden with surfactant contaminated microbubbles. *Chemical Engineering Science* 60 (22), 6176–6187.

Kato, H., Iwashina, T., Miyanaga, M., and Yamaguchi, H., 2000, "Effect of microbubbles on the structure of turbulence in a turbulent boundary layer", *Journal of Marine Science and Technology*, 4 (4), 155–162.

Kim, Kyoungyoun, Baek, Seung-Jin & Sung, Hyung Jin 2002 An implicit velocity decoupling procedure for the incompressible Navier–Stokes equations. *International Journal for Numerical Methods in Fluids* 38 (2), 125–138.

Mathai, Varghese, Lohse, Detlef & Sun, Chao 2020 Bubbly and Buoyant Particle–Laden Turbulent Flows. *Annual Review of Condensed Matter Physics* 11 (1), 529–559.

Molin, D., Marchioli, C., and Soldati, A., 2012, "Turbulence modulation and microbubble dynamics in vertical channel flow", *International Journal of Multiphase Flow* 42, 80-95.

Ortiz-Villafuerte, J., and Hassan, Y. A., 2006, "Investigation of microbubble boundary layer using particle tracking velocimetry", *Journal of Fluids Engineering*, 128, 507–519.

Park, H. J., Saito, D., Tasaka, Y., and Murai, Y., 2019, "Color-coded visualization of microbubble clouds interacting with eddies in a spatially developing turbulent boundary layer", *Experimental Thermal and Fluid Science*, 109, 109919.

Renard, Nicolas & Deck, S´ebastien 2016 A theoretical decomposition of mean skin friction generation into physical phenomena across the boundary layer. *Journal of Fluid Mechanics* 790, 339–367.

Schiller, L. & Naumann, A. 1935 A drag coefficient correlation. *Zeitschrift des Vereins Deutscher Ingenieure* 77, 318–320.